Journal of Asian Earth Sciences 143 (2017) 39–44

Contents lists available at ScienceDirect

Journal of Asian Earth Sciences

journal homepage: www.elsevier.com/locate/jseaes

Full length Article

The Preboreal-like Asian monsoon climate in the early last interglacial period recorded from the Dark Cave, Southwest China

Xiuyang Jiang[a,b], Yaoqi He[c], Xiaoyan Wang[a], Xiaoshuang Sun[a], Hui Hong[a], Juan Liu[d], Tsai-Luen Yu[e], Zhizhong Li[a,b], Chuan-Chou Shen[e,*]

[a] Key Laboratory of Humid Subtropical Eco-geographical Processes, Ministry of Education, College of Geography Science, Fujian Normal University, Fuzhou 350007, China
[b] Institute of Geography, Fujian Normal University, Fuzhou 350007, China
[c] College of Tourism and Air Service, Guizhou Minzu University, Guiyang 550025, China
[d] Innovation Center and Key Laboratory of Waters Safety & Protection in the Pearl River Delta, Ministry of Education, Guangzhou University, Guangzhou 510006, China
[e] High-Precision Mass Spectrometry and Environment Change Laboratory (HISPEC), Department of Geosciences, National Taiwan University, Taipei 106, Taiwan, ROC

ARTICLE INFO

Keywords:
Asian summer monsoon
Dark Cave
Stalagmite
The last interglacial
Preboreal

ABSTRACT

Transitions of glacial-interglacial cycles are critical periods for Quaternary climate shifts. Here, we present new, decadal resolution Asian summer monsoon (ASM) record from three stalagmites obtained from the Dark Cave in southwestern China over 130–114 thousand years ago (ka, before CE 1950). Chronology was anchored by 28 ^{230}Th dates with typical uncertainties of ± 0.3–1.0 kyr, allowing an assessment of timing and transition of climate changes during the onset and end of the last interglacial. An agreement between this new and previous stalagmite δ^{18}O records supports that summer insolation predominates orbital-scale ASM evolution. A 2–3 kyr-long gradually increasing ASM period, analogous to the classical Preboreal episode in the early Holocene, follows the termination of a weak monsoon interval at 129.0 ± 0.8 ka. This finding suggests a strong influence of high-latitude ice-sheet dynamics on Asian monsoonal conditions during the early interglacial period. An abrupt end of the marine isotope stage 5e at 118.8 ± 0.6 ka was probably caused by the internal climate system threshold effects.

1. Introduction

The Asian summer monsoon (ASM), an important component of the global climate system, links to the changes in ice sheet, oceanic and atmospheric circulation, and high-latitude climates (An, 2000; Wang et al., 2001; Cai et al., 2006; Partin et al., 2007, 2015; Liu et al., 2008; Cheng et al., 2009; An et al., 2011). The last interglacial ASM history provides a good reference for in-depth understanding of natural climate variability in the Holocene, the current interglacial period (Xiao et al., 1999; Porter, 2001; Burns et al., 2001; Chen et al., 2003; Yuan et al., 2004; Oppo and Sun, 2005; Kelly et al., 2006; Peterse et al., 2014). Well-dated proxy records have unequivocally shown that ASM conditions of both the last interglacial and the Holocene were dominantly governed by precessional insolation changes (Yuan et al., 2004; Kelly et al., 2006; Wang et al., 2008; Dong et al., 2010; Cai et al., 2010), in support of model simulations (Kutzbach, 1981; Liu et al., 2014).

Previously Chinese speleothem studies reported a similar two-phase glacial termination process, a several millennia of the weak monsoon interval and a rapid increase in monsoon intensity, at the last seven ice ages (Cheng et al., 2006, 2009, 2016). During phase I, a close connection between ice-sheet melting and weak monsoon was revealed (Cheng et al., 2009). During phase II, the southern hemisphere/tropical warming induces a rapid intensification of the ASM (Cheng et al., 2009). The evidence suggests that prior to the commence of interglacial periods, ASM has some common features associated with changes in ice sheets and other climate boundary conditions. However, little is known about similarity between the latest two interglacials. The climate stability of marine isotope stage (MIS) 5e, the last interglacial plateau, has been controversially reported (*e.g.*, Frogley et al., 1999; Rioual et al., 2001). After the interglacial plateau, ASM declined abruptly (Yuan et al., 2004; Kelly et al., 2006 and references therein). Only few records were used to address the detailed physical process (Burns et al., 2015). Additional continuous records with robust chronology are needed to clarify the entire ASM evolution over the last interglacial for further understanding current monsoon dynamics and for envisaging possible future.

Here, we reconstructed a decadal-resolved variability of δ^{18}O record during 130–114 ka of three stalagmites collected from Dark Cave,

* Corresponding author at: HISPEC, Department of Geosciences, National Taiwan University, Taipei, Taiwan, ROC.
E-mail address: river@ntu.edu.tw (C.-C. Shen).

http://dx.doi.org/10.1016/j.jseaes.2017.03.031
Received 22 November 2016; Received in revised form 22 March 2017; Accepted 26 March 2017
Available online 29 March 2017
1367-9120/

southwestern China. With the precisely dated $\delta^{18}O$ record, we show a gradual Preboreal-like (PB-like) ASM increase after the Termination II (T II) and a two-step millennial-scale decreasing trend of ASM intensity during the end of MIS 5e.

2. Study site, materials and methods

Dark Cave (106°10′E, 27°12′N; 1100 m above sea level) is located in Guizhou Province, Southwest China. This 10 km-long cave, with only one entrance, is approximately 270 km northwest of Dongge Cave and 600 km southwest of Sanbao Cave (Fig. 1). A 30–50 cm-thick layer, mainly composed of yellow[1] and calcareous soils, overlies the top of the limestone cave. The well-developed vegetation consists of subtropical broadleaf evergreen and deciduous mixed forests. Modern regional climate conditions have previously been reported by Jiang et al. (2013). The climate is strongly affected by the ASM. Four fifths of the annual rainfall occurs during rainy season from May to October when the convective monsoon rainfall prevails, with less than 20% from November to April.

Stalagmites D13, D14, and D17 were collected 2 km from the entrance. Intact samples D13 and D14 were found partly buried in clay-rich silt. Stalagmite D13 is 717 mm in length and only the uppermost 325-mm was used. D14 is 696 mm in length and with a brown detrital laminae at 112 mm from the top, probably indicating growth discontinuities. D17 was broken when collected. It is 1168 mm long with two clay bands at 40 and 960 mm from the top.

After halved and polished, 28 subsamples, ~60 mg each, were drilled from different layers on a class-100 clean bench in a class-10,000 subsampling clean room to avoid possible contamination (Shen et al., 2003). Procedure for chemical separation and purification of uranium and thorium was described in Shen et al. (2002, 2003). U-Th isotopic analyses were performed on a Thermo-Fisher NEPTUNE multi-collection inductively coupled plasma mass spectrometer (MC-ICP-MS) at the High-Precision Mass Spectrometry and Environment Change Laboratory (HISPEC), Department of Geosciences, National Taiwan University (Shen et al., 2012). Half-lives of U-Th nuclides used for ^{230}Th age calculation are given in Cheng et al. (2013). Isotopic and age errors given are two standard deviation of the mean and two standard deviation, respectively, unless otherwise noted.

For $\delta^{18}O$ measurements, subsamples were milled along a profile parallel to the central growth axis. A total of 866 subsamples, 50–100 μg each, were analyzed using a Thermo-Fisher MAT-253 isotope ratio mass spectrometer equipped with an automated carbonate preparation system (Gasbench II) at the College of Geography Science, Fujian Normal University. Results are reported relative to the Vienna Pee Dee Belemnite (VPDB) standard and standardization was accomplished using NBS-19. Precision of $\delta^{18}O$ values is ± 0.06‰ at the 1-sigma level.

3. Results and discussion

3.1. Chronology

Uranium and thorium isotopic compositions and ^{230}Th dates are listed in Table 1. For stalagmite D13, ^{238}U ($[^{238}U]$) and $[^{232}Th]$ contents are 0.4–0.6 ppm and 0.3–14 ppb, respectively. Uncertainty of corrected ^{230}Th dates ranges from ± 0.4 to ± 1.0 kyr. The growth interval is from 115 to 130 ka. $[^{238}U]$ of stalagmite D14 is relatively high, ranging from 0.8–1.2 ppm, and $[^{232}Th]$ 2.2–38.8 ppb. The ^{230}Th dates are yielded with errors of ± 0.3–0.9 ka. The growth interval is from 114 to 124 ka. For stalagmite D17, $[^{238}U]$ is 0.6–0.9 ppm and $[^{232}Th]$ 0.2–2.2 ppb. Precision of the corrected ^{230}Th dates is ± 0.3–0.6 kyr.

[1] For interpretation of color in Fig. 1, the reader is referred to the web version of this article.

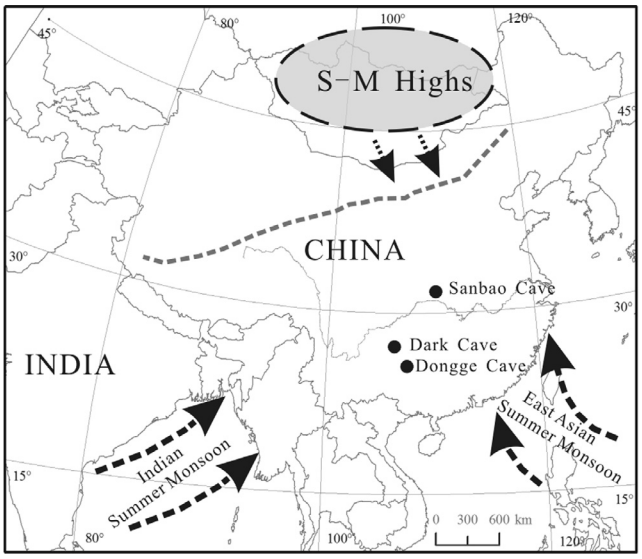

Fig. 1. Location of Sanbao Cave (Wang et al., 2008); Dongge Cave (Kelly et al., 2006) and Dark Cave (this study). Dashed line represents the average modern ASM limit. Elliptical area denotes the position of the Siberian-Mongolian Highs (S-M Highs).

This stalagmite grew from 123 to 128 ka.

Age-depth plots for the study segments of three stalagmites are illustrated in Fig. 2. All ^{230}Th ages are in a stratigraphic order. The chronology is developed using linear interpolation between ^{230}Th dates.

3.2. $\delta^{18}O$ record

The well-known Hendy Test (Hendy, 1971) has been taken as an essential requirement when assessing the ability of stalagmites to serve as paleoclimatic archives. The $\delta^{18}O$ and $\delta^{13}C$ data of coeval subsamples from six layers of three stalagmites are plotted in Fig. 3. The 2σ variability of only ± 0.08–0.21‰ for the coeval subsample $\delta^{18}O$ data and the insignificant correlation ($0.02 < r^2 < 0.25$) between $\delta^{18}O$ and $\delta^{13}C$ values indicate that the oxygen data of the selected layers pass the Hendy Test. A correlation test between $\delta^{18}O$ and $\delta^{13}C$ for D13 and D14 reveals a weak relationship ($r^2 = 0.0001$ for D13, 0.002 for D14), that is not statistically significant. The correlation coefficient is relatively high ($r^2 = 0.29$) for only D17. Another critical evaluation for the paleoclimatic suitability of stalagmites is Replication Test of proxy records from different locations within the same cave or between caves (Dorale and Liu, 2009). Contemporaneous $\delta^{18}O$ sequences of three stalagmites, D13, D14, and D17, match each other within age uncertainty (Fig. 4b). Furthermore, orbital-scale variability of dark cave records agrees with ones of Dongge (Kelly et al., 2006) and Sanbao (Wang et al., 2008) Caves, dominated by regional insolation change (Fig. 4). The good replication of $\delta^{18}O$ records between Dark and other Chinese caves indicates that our selected stalagmites deposited under equilibrium conditions. The stalagmite $\delta^{18}O$ data can represent rainfall oxygen isotopic change. Following the previous interpretation, the shifts in Chinese stalagmite $\delta^{18}O$ are generally related to changes of ASM intensity, with lower $\delta^{18}O$ values reflecting stronger ASM and vice versa (Wang et al., 2001, 2008; Yuan et al., 2004; Cheng et al., 2009, 2016; Liu et al., 2010; Zhou et al., 2011; Duan et al., 2014; Dong et al., 2015; Jiang et al., 2016).

Dark Cave stalagmite $\delta^{18}O$ profiles are given in Fig. 4. The $\delta^{18}O$ record, ranging from −4.6‰ to −10.9‰, begins at 130 ka, a period just before the onset of the strong ASM at the last interglacial. The average temporal resolution of $\delta^{18}O$ sequences is 10 yr from 129 to 123 ka and 50 yr from 123 to 114 ka, covering the entire MIS 5e. Our well-established age model shows the ASM T II, a midpoint of the negative shift in $\delta^{18}O$ marking the onset of the last interglacial ASM, at 129.0 ± 0.8 ka, matching previous dates in stalagmite records of

Table 1
^{230}Th dating results for stalagmites D13, D14, and D17, Dark Cave, southwestern China.

Sample number	Depth (cm)	^{238}U (ng/g)	^{232}Th (pg/g)	δ^{234}U (measured)	^{230}Th/^{238}U (activity)	^{230}Th age (a) (Uncorrected)	^{230}Th age (a B.P.) (corrected)	$^{234}U_{Inital}$ (corrected)
D13-15	1.5	442 ± 0.6	766 ± 8	1155 ± 3	1.517 ± 0.005	115,145 ± 679	**115,062 ± 679**	1598 ± 5
D13-45	4.5	427 ± 0.5	2321 ± 10	1129 ± 2	1.503 ± 0.003	115,826 ± 473	**115,704 ± 474**	1565 ± 4
D13-85	8.5	458 ± 0.7	253 ± 8	1111 ± 3	1.510 ± 0.004	118,347 ± 579	**118,276 ± 579**	1552 ± 5
D13-121	12.1	420 ± 0.6	741 ± 8	1090 ± 3	1.501 ± 0.004	119,154 ± 629	**119,070 ± 629**	1526 ± 6
D13-133	13.3	501 ± 0.7	2517 ± 11	1080 ± 3	1.498 ± 0.004	119,940 ± 646	**119,822 ± 646**	1514 ± 5
D13-167	16.7	440 ± 0.6	406 ± 8	1068 ± 3	1.502 ± 0.004	121,648 ± 647	**121,573 ± 647**	1505 ± 5
D13-185	18.5	394 ± 0.6	553 ± 7	1056 ± 3	1.510 ± 0.004	123,899 ± 632	**123,819 ± 632**	1498 ± 5
D13-219	21.9	511 ± 0.8	2734 ± 11	1050 ± 3	1.511 ± 0.004	124,734 ± 663	**124,613 ± 663**	1492 ± 5
D13-237	23.7	475 ± 0.4	6896 ± 15	1043 ± 2	1.509 ± 0.005	125,220 ± 660	**125,001 ± 664**	1484 ± 4
D13-281	28.1	423 ± 0.3	14,109 ± 30	1035 ± 1	1.514 ± 0.007	126,844 ± 982	**126,422 ± 995**	1478 ± 5
D13-323	32.3	634 ± 0.5	2435 ± 8	1027 ± 2	1.530 ± 0.002	130,057 ± 384	**129,951 ± 384**	1482 ± 3
D14-120	12.0	848 ± 1.2	12,241 ± 24	1234 ± 3	1.568 ± 0.005	114,107 ± 659	**113,900 ± 662**	1703 ± 6
D14-212	21.2	1120 ± 1.2	2152 ± 10	1246 ± 2	1.588 ± 0.002	115,419 ± 340	**115,335 ± 340**	1726 ± 4
D14-410	41.0	1013 ± 1.0	1366 ± 8	1233 ± 2	1.615 ± 0.002	119,824 ± 352	**119,745 ± 352**	1729 ± 3
D14-515	51.5	1130 ± 1.0	38,802 ± 108	1226 ± 2	1.616 ± 0.007	120,559 ± 875	**120,160 ± 888**	1721 ± 5
D14-560	56.0	1159 ± 1.2	8099 ± 17	1229 ± 2	1.631 ± 0.003	122,080 ± 436	**121,948 ± 437**	1734 ± 4
D14-598	59.8	1128 ± 1.0	31,659 ± 75	1215 ± 2	1.626 ± 0.006	122,858 ± 720	**122,520 ± 732**	1717 ± 5
D14-635	63.5	1207 ± 1.1	11,759 ± 25	1214 ± 2	1.628 ± 0.004	123,205 ± 507	**123,045 ± 508**	1718 ± 3
D14-690	69.0	1203 ± 1.1	3375 ± 10	1212 ± 2	1.635 ± 0.003	123,998 ± 381	**123,906 ± 381**	1722 ± 3
D17-50	5.0	761 ± 0.6	165 ± 9	1218 ± 2	1.632 ± 0.002	123,321 ± 325	**123,254 ± 325**	1725 ± 3
D17-56	5.6	745 ± 0.6	401 ± 9	1216 ± 2	1.632 ± 0.003	123,459 ± 437	**123,389 ± 437**	1723 ± 3
D17-233	23.3	850 ± 0.7	1592 ± 10	1222 ± 2	1.646 ± 0.003	124,684 ± 361	**124,601 ± 361**	1737 ± 3
D17-449	44.9	953 ± 0.8	2197 ± 10	1204 ± 2	1.635 ± 0.003	124,945 ± 361	**124,857 ± 361**	1713 ± 3
D17-487	48.7	881 ± 0.7	1206 ± 10	1201 ± 1	1.635 ± 0.002	125,273 ± 322	**125,194 ± 322**	1710 ± 3
D17-685	68.5	654 ± 0.6	189 ± 10	1200 ± 2	1.642 ± 0.003	126,310 ± 397	**126,242 ± 397**	1714 ± 3
D17-767	76.7	965 ± 0.8	544 ± 10	1209 ± 2	1.651 ± 0.002	126,536 ± 314	**126,465 ± 314**	1728 ± 3
D17-943	94.3	558 ± 0.7	1499 ± 10	1240 ± 3	1.685 ± 0.004	127,675 ± 620	**127,585 ± 620**	1778 ± 6
D17-955	95.5	592 ± 0.8	519 ± 9	1239 ± 3	1.687 ± 0.004	128,129 ± 620	**128,055 ± 620**	1779 ± 5

Corrected ^{230}Th ages are indicated in bold. Errors are 2σ analytical errors. Decay constant values are $\lambda_{230} = 9.1705 \times 10^{-6}\ yr^{-1}$, $\lambda_{234} = 2.82206 \times 10^{-6}\ yr^{-1}$, $\lambda_{238} = 1.55125 \times 10^{-10}\ yr^{-1}$. Corrected ^{230}Th ages assume an initial ^{230}Th/^{232}Th atomic ratio of $(4 \pm 2) \times 10^{-6}$. All corrected dates are presented in the year before 1950 CE.

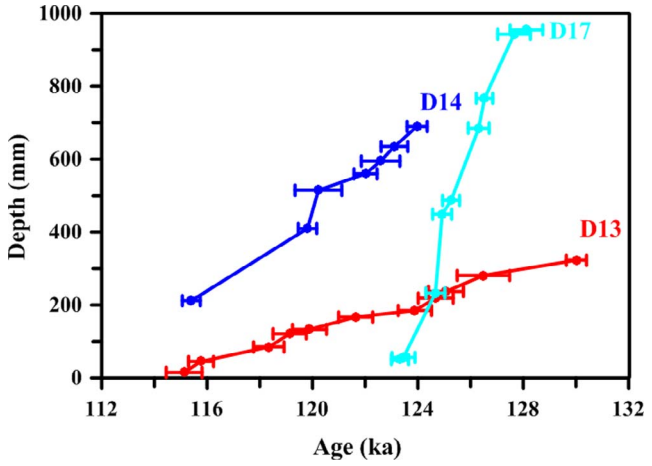

Fig. 2. The age-depth profiles for stalagmites D13, D14, and D17. The dots depict positions for the dated subsamples. Horizontal bars are dating errors.

Dongge Cave in southern China (Kelly et al., 2006) and of Sanbao Cave in central China (Cheng et al., 2009) within dating errors. Subsequently, δ^{18}O values decreased slowly from −8.2 to −10.5‰ during 129.0–126.5 ka.

The range of decadal-resolved δ^{18}O data of Dark Cave stalagmites is from −10.9 to −9.3‰, with a typical amplitude of somewhat 0.6–1.4‰, during the last interglacial plateau from 126.5 to 122 ka (Fig. 4). The clear multi-decadal to centennial-scale shifts in δ^{18}O indicates the presence of high-frequency oscillations of the ASM at MIS 5e. This variability is also recorded in the Chinese Holocene stalagmites (Wang et al., 2005; Hu et al., 2008; Dong et al., 2010; Jiang et al., 2013; Zhao et al., 2016). The consistency suggests this multi-decadal to centennial-scale variability is one of intrinsic characteristics of interglacial ASM.

After this ASM interglacial plateau, the stalagmite δ^{18}O data slowly increase from −10.5‰ at 122.0 ka to −8.7‰ at 119.0 ka and then abruptly rise to −6.5‰ at 118.8 ± 0.6 ka. The age of the end of MIS 5e also matches previous ones in stalagmite records of Dongge (Kelly et al., 2006) and Sanbao (Wang et al., 2008) Caves within dating errors.

3.3. The Preboreal-like early last interglacial

Before approaching the Holocene Optimum, the ASM experienced a 2.6 kyr-long gradual enhancement during 11.5–8.9 ka in Sanbao records (Fig. 5a, Dong et al., 2010), called the Preboreal (PB) chronozone (Wanner et al., 2008). The gradual trend of PB ASM enhancement is also observed in other ASM records of Dongge Cave (Dykoski et al., 2005), Qunf Cave (Fleitmann et al., 2003), and Mawmluch Cave (Dutt et al., 2015). After an abruptly T II transition at 129.0 ka, our new Dark Cave record is marked by a millennial-scale decreasing δ^{18}O of 2.3‰, from −8.2‰ at 129.0 ka to −10.5‰ at 126.5 ka, before reaching MIS 5e ASM optimum (Fig. 5b). It expresses a 2.5-kyr PB-like ASM intensification process (Fig. 5b), matching the observation in Sanbao and Dongge records within dating errors (Fig. 4, Wang et al., 2008). Stalagmite δ^{18}O data from Sanbao Cave also show that the 2.5-kyr PB-like ASM enhancement occurred after T III and T IV (Fig. 5c and d; Cheng et al., 2009). This remarkable resemblance suggests that the ASM conditions during the early interglacial periods could be governed by similar forcing(s).

The onset of optimum interglacial conditions at 126.5 ± 0.3 ka shown in Dark Cave record is in agreement with the beginning of the marine MIS 5e plateau, as identified in benthic δ^{18}O records (e.g., Shackleton et al., 2002, 2003), the global mean age of 126 ± 1.7 ka for the beginning of the last interglacial sea level high stand (Fig. 5b, Waelbroeck et al., 2008), and the Greenland temperature peak at 126 ka (Fig. 5b, NEEM community members, 2013). According to the ice-volume equivalent sea level (Lambeck and Chappell, 2001), we

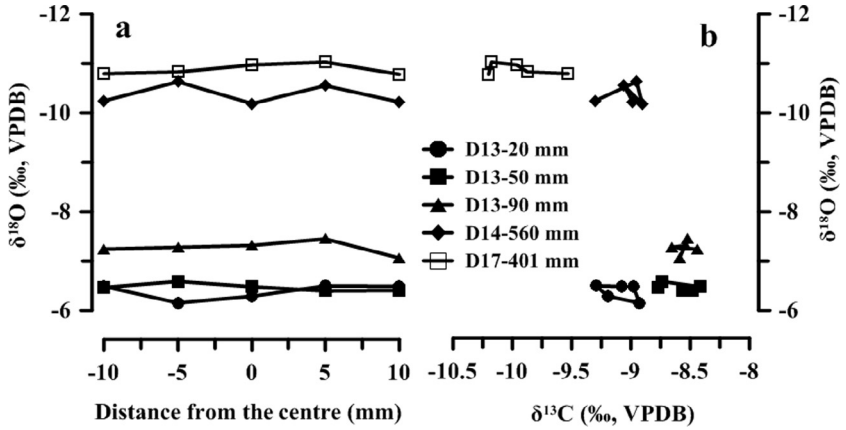

Fig. 3. Results of the Hendy Test at arbitrarily selected six growth layers of three stalagmites, D13, D14, and D17. (a) Two-sigma variability on the same growth layers varies between ± 0.08–0.21‰ for $\delta^{18}O$. (b) Plots of $\delta^{18}O$ versus $\delta^{13}C$ for coeval subsamples.

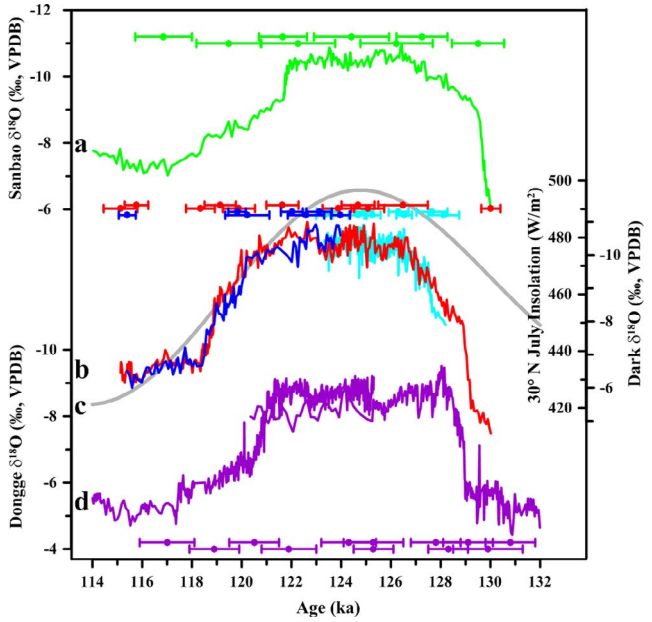

Fig. 4. Comparison of stalagmite $\delta^{18}O$ records between caves of (a) Sanbao (Wang et al., 2008), (b) Dark (this study), and (d) Dongge (Kelly et al., 2006). (c) 30°N July summer insolation (Berger and Loutre, 1991). ^{230}Th dates and 2wo-sigma errors are color-coded by stalagmite.

propose that the 2.5-kyr PB-like ASM intensification could be related to the glacial boundary conditions. A threshold of the global ice volume occurs at benthic foraminiferal $\delta^{18}O$ value of 3.4‰ (Fig. 5), corresponding to a sea level of ~30 m below present (Lisiecki and Raymo, 2005). When the benthic foraminiferal $\delta^{18}O$ value large than 3.4‰ before the interglacial Optimum, a large remnant ice sheet during the PB-like period in the Northern Hemisphere may outcompete the summer insolation on influencing the strength of the ASM (Wanner et al., 2008).

After the major transition of past four terminations, the large remnant ice sheet still covered the North Hemisphere during the PB-like periods (Fig. 5) (Lisiecki and Raymo, 2005), preventing ocean heat from low latitudes to extremely cold Eurasia, which would result in a southward shift of the Intertropical Convergence Zone (ITCZ) over the Atlantic and the Pacific (Chiang and Bitz, 2005), and consequently decelerating the ASM rebound through air-sea interactions (Zhang and Delworth, 2005). Our results suggest global ice volume is one of important forcings on ASM intensity during the early interglacial periods. The gradual ASM enhancement at PB and PB-like intervals were mainly influenced by the glacial boundary conditions (Fleitmann et al., 2003; Wanner et al., 2008; Törnqvist and Hijma, 2012).

3.4. The end of the MIS 5e

The ending transition of ASM optimum at MIS 5e in Dark Cave record is marked by a two-step 3.2-kyr pattern from 122.0 to 118.8 ka (Fig. 6). The stalagmite $\delta^{18}O$ data slowly increase from −10.5‰ at 122.0 ka to −8.7‰ at 119.0 ka and then abruptly rise to −6.5‰ at 118.8 ka. However, the $\delta^{18}O$ in Sanbao (Fig. 4a) and Dongge (Fig. 4c) caves show a 100-yr abrupt increase and then a gradual increase at the following several thousands years (Wang et al., 2008; Kelly et al., 2006). This insignificant difference between Dark and other Chinese cave records is within errors (Fig. 4). At this time interval, a robust age model in Dark Cave record, determined with six precise ^{230}Th dates and an averaged uncertainty of ± 0.6 kyr, provides a relatively solid ASM structure. The end of the MIS 5e is precisely dated to be 118.8 ± 0.6 ka in Dark Cave, consistent with speleothem records in European Alps at 118 ± 2 ka (Meyer et al., 2008) and in the eastern Mediterranean at 119 ± 3 ka (Bar-Matthews et al., 2003).

Although insolation predominates orbital-scale ASM evolution (Wang et al., 2008; Cheng et al., 2016), a 2-step decrease in ASM intensity at 122 ka inferred from Dark Cave record lags insolation decrease at 125 ka by a few thousand years (Fig. 6). We speculate that the difference of this 2-step ending transition from insolation change implies a possible nonlinear ASM response to insolation on sub-orbital scale (Fig. 6). Additional internal factors of global climate system might be involved. The cooling of the high northern latitudes at ~121 ka (Fig. 6, NEEM community members, 2013) could strengthen the East Asian winter monsoon circulation through enhancing the Westerly zone and Siberian cold high-pressure (Denton et al., 2005) and causing the southern migration of the ITCZ (Chiang and Friedman, 2012). Kelly et al. (2006) firstly proposed that under a certain threshold condition, an abrupt ASM decrease could be triggered to determinate the MIS 5e. The physical processes have not been clarified and further proxy records and model simulations are required.

4. Conclusions

Comparison of the last interglacial stalagmite-based oxygen isotope profiles between Dark and other Chinese caves provides detailed spatiotemporal ASM variability. The results show a three-phase ASM evolution during the last interglacial, characterized with a 2–3 kyr gradual transition, a 4.5-kyr prevailing ASM plateau, and a 3-kyr reducing in the ASM intensity. Agreement between this new and previous stalagmite $\delta^{18}O$ records supports that summer insolation predominates orbital-scale ASM evolution. After the abrupt transition of the T II at 129.0 ± 0.8 ka, the gradual ASM enhancement at the PB-

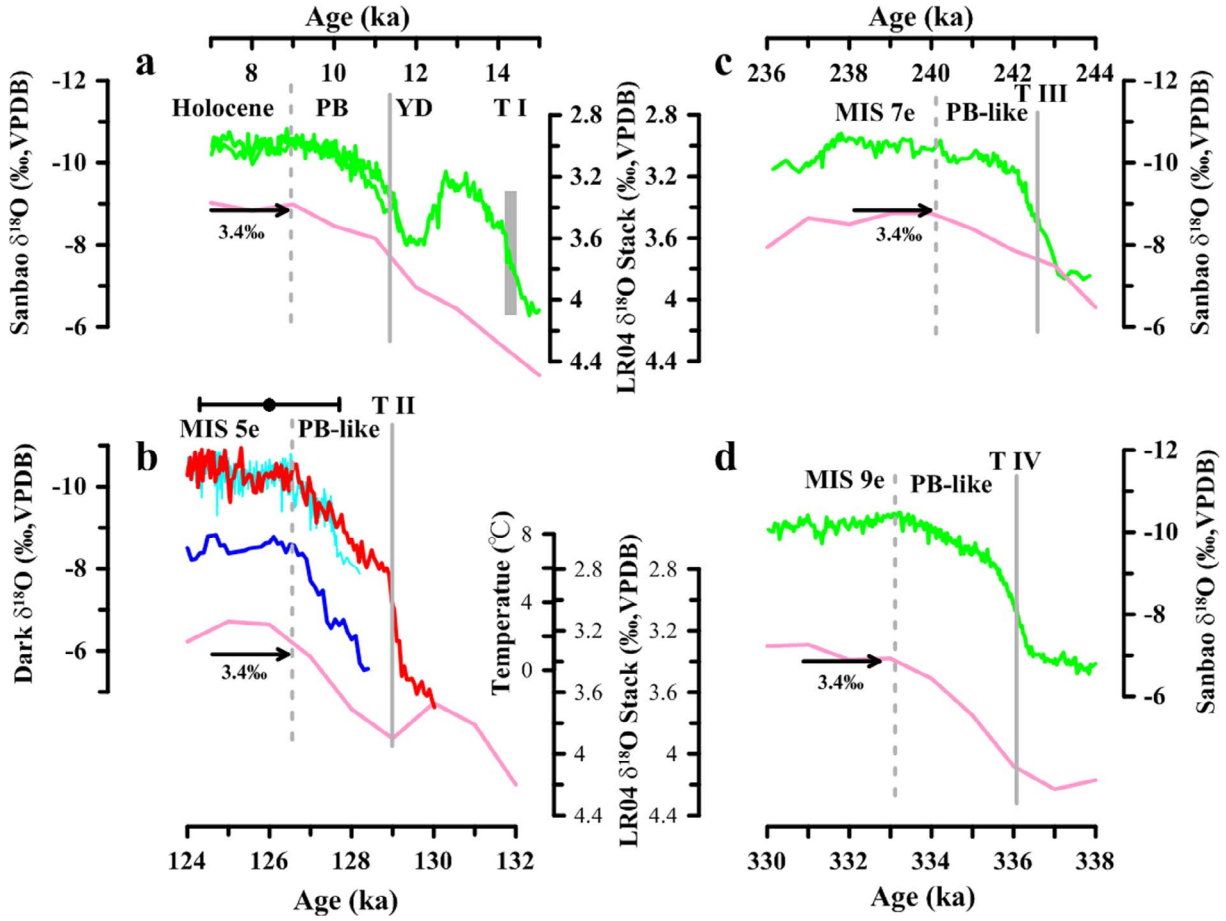

Fig. 5. Comparison of the ASM variability across the last four glacial/interglacial transitions (a–d). Green line denotes Sanbao Cave $\delta^{18}O$ record (Dong et al., 2010; Cheng et al., 2009), pink line LR04 benthic foraminiferal $\delta^{18}O$-inferred global ice volume curve (Lisiecki and Raymo, 2005), and red and cyan curves Dark Cave $\delta^{18}O$ records. Blue line denotes NEEM temperature record (NEEM Project members, 2013). A ^{230}Th age with error bar given in b represents the beginning of marine MIS 5e (Shackleton et al., 2002, 2003). Solid and dash lines highlight the major transitions and the onset of the interglacial Optimum, respectively. A critical value of 3.4‰ in LR04 record (Lisiecki and Raymo, 2005) represents an important threshold in ice sheet melting (see text). (For interpretation of the references to color in this figure legend, the reader is referred to the web version of this article.)

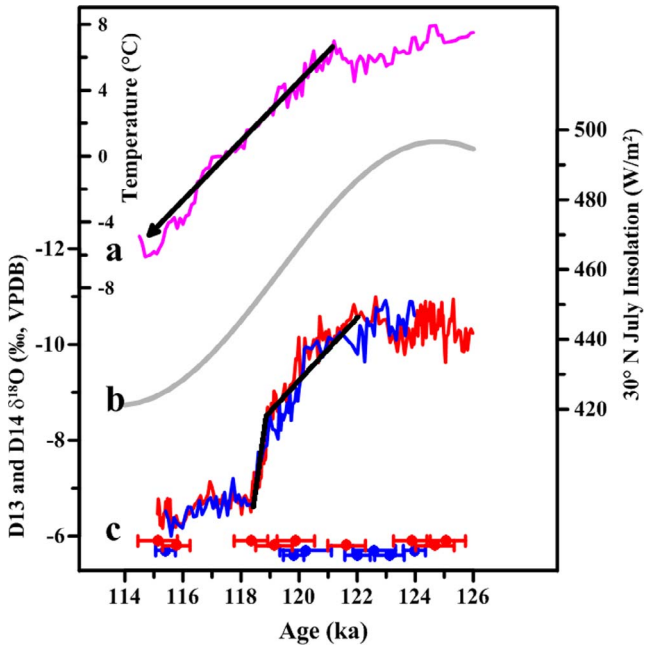

Fig. 6. Comparison among Dark Cave $\delta^{18}O$ record, NEEM temperature, and insolation. (a) NEEM temperature record (magenta curve, NEEM Project members, 2013). (b) 30°N July insolation (gray curve, Berger and Loutre, 1991). (c) Dark Cave $\delta^{18}O$ records (blue and red curves). Records are plotted on their own timescales. (For interpretation of the references to color in this figure legend, the reader is referred to the web version of this article.)

like interval suggests that the ASM rainfall is probably imprinted by the glacial boundary conditions at the early last interglacial. Dark Cave record is also exhibited with a two-step ASM decreasing trend from 122.0 to 118.8 ka before approaching a weak ASM realm.

Acknowledgments

We thank Dr. Yongjin Wang of the Nanjing Normal University for instructive comments. This study was jointly supported by grants of the National Natural Science Foundation of China (Grant Nos. 41372189, 41463014 and 41672170), Natural Science Foundation of Fujian Province (Grant No. 2017J01654), and the Outstanding Youth Scientific Research Program in Fujian Province University. Funding was also provided by grants from Taiwan ROC MOST (104-2119-M-002-003 and 105-2119-M-002-001 to C.-C.S.) and the National Taiwan University (105R7625 to C.-C.S.).

References

An, Z., Clemens, S.C., Shen, J., Qiang, X., Jin, Z., Sun, Y., Prell, W.L., Luo, J., Wang, S., Xu, H., Cai, Y., Zhou, W., Liu, X., Liu, W., Shi, Z., Yan, L., Xiao, X., Chang, H., Wu, F., Ai, L., Lu, F., 2011. Glacial-interglacial Indian summer monsoon dynamics. Science 333, 719–723.

An, Z.S., 2000. The history and variability of the East Asian paleomonsoon climate. Quatern. Sci. Rev. 19, 171–187.

Bar-Matthews, M., Ayalon, A., Gilmour, M., Matthews, A., Hawkesworth, C.J., 2003. Sea-land oxygen isotopic relationships from planktonic foraminifera and speleothems in the Eastern Mediterranean region and their implication for paleorainfall during interglacial intervals. Geochim. Cosmochim. Acta 67, 3181–3199.

Berger, A., Loutre, M.F., 1991. Insolation values for the climate of the last 10 million years. Quatern. Sci. Rev. 10, 297–317.
Burns, S.J., Fleitmann, D., Matter, A., Neff, U., Mangini, A., 2001. Speleothem evidence from Oman for continental pluvial events during interglacial periods. Geology 29, 623–626.
Burns, S.J., Kanner, L.C., Cheng, H., Edwards, R.L., 2015. A tropical speleothem record of glacial inception, the South American summer monsoon from 125 to 115 ka. Climate Past 11, 931–938.
Cai, Y., An, Z., Cheng, H., Edwards, R.L., Kelly, M.J., Liu, W., Wang, X., Shen, C.-C., 2006. High-resolution absolute-dated Indian monsoon record between 53 and 36 ka from Xiaobailong Cave, southwestern China. Geology 34, 621–624.
Cai, Y.J., Cheng, H., An, Z.S., Edwards, R.L., Wang, X.F., Tan, L.C., Wang, J., 2010. Large variations of oxygen isotope in precipitation over south-central Tibet during marine isotope stage 5. Geology 38, 243–246.
Chen, F.H., Qiang, M.R., Feng, Z.D., Wang, H.B., Bloemendal, J., 2003. Stable East Asian monsoon climate during the Last Interglacial (Eemian) indicated by paleosol S1 in the western part of the Chinese Loess Plateau. Global Planet. Change 36, 171–179.
Cheng, H., Edwards, R.L., Broecker, W.S., Denton, G.H., Kong, X., Wang, Y., Zhang, R., Wang, X., 2009. Ice age terminations. Science 326, 248–252.
Cheng, H., Edwards, R.L., Kong, X.G., Ming, Y.F., Kelly, M.J., Wang, X.F., Gallup, C.D., Liu, W.G., 2006. A penultimate glacial monsoon record from Hulu Cave and two-phase glacial terminations. Geology 34, 217–220.
Cheng, H., Edwards, R.L., Sinha, A., Spötl, C., Yi, L., Chen, S.T., Kelly, M., Kathayat, G., Wang, X.F., Li, X.L., Kong, X.G., Wang, Y.J., Ning, Y.F., Zhang, H.W., 2016. The Asian monsoon over the past 640,000 years and ice age terminations. Nature 534, 640–646.
Cheng, H., Edwards, R.L., Shen, C.-C., Polyak, V.J., Asmerom, Y., Woodhead, J., Hellstrom, J., Wang, Y.J., Kong, X.G., Spötl, C., Wang, X.F., Alexander, E.C., 2013. Improvements in ^{230}Th dating, ^{230}Th and ^{234}U half-life values, and U-Th isotopic measurements by multi-collector inductively coupled plasma mass spectrometry. Earth Planet. Sci. Lett. 372, 82–91.
Chiang, J.H., Bitz, C., 2005. Influence of high latitude ice cover on the marine Intertropical Convergence Zone. Clim. Dyn. 25, 477–496.
Chiang, J.C.H., Friedman, A.R., 2012. Extratropical cooling, interhemispheric thermal gradients, and tropical climate change. Annu. Rev. Earth Planet. Sci. 40, 383–412.
Denton, G.H., Alley, R.B., Comer, G.C., Broecker, W.S., 2005. The role of seasonality in abrupt climate change. Quatern. Sci. Rev. 24, 1159–1182.
Dong, J.G., Shen, C.-C., Kong, X.G., Wang, H.-C., Jiang, X.Y., 2015. Reconciliation of hydroclimate sequences from the Chinese Loess Plateau and low-latitude East Asian summer monsoon regions over the past 14,500 years. Palaeogeogr. Palaeoclimatol. Palaeoecol. 435, 127–135.
Dong, J.G., Wang, Y.J., Cheng, H., Hardt, B., Edwards, R.L., Kong, X.G., Wu, J.Y., Chen, S.T., Liu, D.B., Jiang, X.Y., Zhao, K., 2010. A high-resolution stalagmite record of the Holocene East Asian monsoon from Mt Shennongjia, central China. Holocene 20 (2), 257–264.
Dorale, J.A., Liu, Z., 2009. Limitations of Hendy test criteria in judging the paleoclimate suitability of speleothems and the need for replication. J. Cave Karst Stud. 71, 73–80.
Duan, F., Liu, D., Cheng, H., Wang, X., Wang, Y., Kong, X., Chen, S., 2014. A high resolution monsoon record of millennial-scale oscillations during Late MIS 3 from Wulu Cave, south-west China. J. Quat. Sci. 29, 83–90.
Dutt, S., Gupta, A.K., Clemens, S.C., Cheng, H., Singh, R.K., Kathayat, G., Edwards, R.L., 2015. Abrupt changes in Indian summer monsoon strength during 33,800 to 5500 years B.P. Geophys. Res. Lett. 42, 5526–5532. http://dx.doi.org/10.1002/2015GL064015.
Dykoski, C.A., Edwards, R.L., Cheng, H., Yuan, D.X., Cai, Y.J., Zhang, M.L., Lin, Y.S., Qing, J.M., An, Z.S., Revenaugh, J., 2005. A high-resolution, absolute-dated Holocene and deglacial Asian monsoon records from Dongge cave, China. Earth Planet. Sci. Lett. 233, 71–86.
Fleitmann, D., Burns, S.J., Mudelsee, M., Neff, U., Kramers, J., Mangini, A., Matter, A., 2003. Holocene forcing of the Indian monsoon recorded on a stalagmite from southern Oman. Science 300, 1737–1739.
Frogley, M.R., Tzedakis, P.C., Heaton, T.H.E., 1999. Climate variability in northwest Greece during the last interglacial. Science 285, 1886–1889.
Hendy, C.H., 1971. The isotopic geochemistry of speleothems-I. The calculation of the effects of different modes of formation on the isotopic composition of speleothems and their applicability as palaeoclimatic indicators. Geochim. Cosmochim. Acta 35, 801–824.
Hu, C.Y., Henderson, G.M., Huang, J., Xie, S., Sun, Y., Johnson, K.R., 2008. Quantification of Holocene Asian monsoon rainfall from spatially separated cave records. Earth Planet. Sci. Lett. 266, 221–232.
Jiang, X., He, Y., Shen, C.-C., Li, Z.Z., Lin, K., 2013. Replicated stalagmite-inferred centennial- to decadal-scale monsoon precipitation variability in southwest China since the mid Holocene. Holocene 23, 848–856.
Jiang, X.Y., Wang, X.Y., He, Y.Q., Hu, H.-M., Li, Z.Z., Spötl, C., Shen, C.-C., 2016. Precisely dated multidecadally resolved Asian summer monsoon dynamics 113.5–86.6 thousand years ago. Quatern. Sci. Rev. 143, 1–12.
Kelly, M.J., Edwards, R.L., Cheng, H., Yuan, D.X., Zhang, M.L., An, Z.S., 2006. High resolution characterization of the AM between 146,000 and 99,000 years B.P. from Dongge Cave, China and global correlation of events surrounding Termination II. Palaeogeogr. Palaeoclimatol. Palaeoecol. 236, 20–38.
Kutzbach, J.E., 1981. Monsoon climate of the early Holocene: climate experiment with Earth's orbital parameters for 9000 years ago. Science 214, 59–61.
Lambeck, K., Chappell, J., 2001. Sea level change through the last glacial cycle. Science 292, 679–686.
Lisiecki, L.E., Raymo, M.E., 2005. A Pliocene-Pleistocene stack of 57 globally distributed benthic δ^{18}O records. Paleoceanography 20, PA1003. http://dx.doi.org/10.1029/2004PA001071.
Liu, D., Wang, Y., Cheng, H., Edwards, R.L., Kong, X., Wang, X., Wu, J., Chen, S., 2008. A detailed comparison of Asian monsoon intensity and Greenland temperature during the Allerød and Younger Dryas events. Earth Planet. Sci. Lett. 272, 691–697.
Liu, D., Wang, Y., Cheng, H., Edwards, R.L., Kong, X., Wang, X., Hardt, B., Wu, J., Chen, S., Jiang, X., He, Y., Dong, J., Zhao, K., 2010. Sub-millennial variability of Asian monsoon intensity during the early MIS 3 and its analogue to the ice age terminations. Quatern. Sci. Rev. 29, 1107–1115.
Liu, Z., Wen, X., Brady, E.C., Otto-Bliesner, B., Yu, G., Lu, H., Cheng, H., Wang, Y., Zheng, W., Ding, Y., Edwards, R.L., Cheng, J., Liu, W., Yang, H., 2014. Chinese cave records and the East Asia summer monsoon. Quatern. Sci. Rev. 83, 115–128.
Meyer, M.C., Spötl, C., Mangini, A., 2008. The demise of the Last interglacial recorded in isotopically dated speleothems from the Alps. Quatern. Sci. Rev. 27, 476–496.
NEEM community members, 2013. Eemian interglacial reconstructed from a Greenland folded ice core. Nature 493, 489–494.
Oppo, D.W., Sun, Y.B., 2005. Amplitude and timing of sea-surface temperature change in the northern South China Sea: dynamic link to the East Asian monsoon. Geology 33, 785–788.
Partin, J.W., Cobb, K.M., Adkins, J.F., Clark, B., Fernandez, D.P., 2007. Millennial-scale trends in west Pacific warm pool hydrology since the Last Glacial Maximum. Nature 449, 452–455.
Partin, J.W., Quinn, T.M., Shen, C.-C., Okumura, Y., Cardenas, M.B., Siringan, F.P., Banner, J.L., Lin, K., Hu, H.-M., Taylor, F.W., 2015. Gradual onset and recovery of the Younger Dryas abrupt climate event in the tropics. Nat. Commun. 6, 8061. http://dx.doi.org/10.1038/ncomms9061.
Peterse, F., Martinez-Garcia, A., Zhou, B., Beets, C.J., Prins, M.A., Zheng, H.B., Eglinton, T., 2014. Molecular records of continental air temperature and monsoon precipitation variability in East Asia spanning the past 130,000 years. Quatern. Sci. Rev. 83, 76–82.
Porter, S.C., 2001. Chinese loess record of monsoon climate during the last glacial–interglacial cycle. Earth Sci. Rev. 54, 115–128.
Rioual, P., Andrieu-Ponel, V., Rietti-Shati, M., Battarbee, R.W., de Beaulieu, J.-L., Cheddadi, R., Reille, M., Svobodova, H., Shemesh, A., 2001. High-resolution record of climate stability in France during the last interglacial period. Nature 413, 293–296.
Shackleton, N.J., Chapman, M., Sánchez-Goñi, M.F., Pailler, D., Lancelot, Y., 2002. The classic marine isotope substage 5e. Quatern. Res. 58, 14–16.
Shackleton, N.J., Sánchez-Goñi, M.F., Pailler, D., Lancelot, Y., 2003. Marine isotope substage 5e and the Eemian interglacial. Global Planet. Change 36, 151–155.
Shen, C.-C., Cheng, H., Edwards, R.L., Moran, S.B., Edmonds, H.N., Hoff, J.A., Thomas, R.B., 2003. Measurement of attogram quantities of ^{231}Pa in dissolved and particulate fractions of seawater by isotope dilution thermal ionization mass spectroscopy. Anal. Chem. 75, 1075–1079.
Shen, C.-C., Lawrence Edwards, R., Cheng, H., Dorale, J.A., Thomas, R.B., Bradley Moran, S., Weinstein, S.E., Edmonds, H.N., 2002. Uranium and thorium isotopic and concentration measurements by magnetic sector inductively coupled plasma mass spectrometry. Chem. Geol. 185, 165–178.
Shen, C.-C., Wu, C.-C., Cheng, H., Edwards, R.L., Hsieh, Y.-T., Gallet, S., Chang, C.-C., Li, T.-Y., Lam, D.D., Kano, A., Hori, M., Spotl, C., 2012. High-precision and high-resolution carbonate ^{230}Th dating by MC-ICP-MS with SEM protocols. Geochim. Cosmochim. Acta 99, 71–86.
Törnqvist, T.E., Hijma, M.P., 2012. Links between early Holocene ice-sheet decay, sea-level rise and abrupt climate change. Nat. Geosci. 5, 601–606.
Waelbroeck, C., Frank, N., Jouzel, J., Parrenin, F., Masson-Delmotte, V., Genty, D., 2008. Transferring radiometric dating of the last interglacial sea level high stand to marine and ice core records. Earth Planet. Sci. Lett. 265, 183–194.
Wang, Y.J., Cheng, H., Edwards, R.L., An, Z.S., Wu, J.Y., Shen, C.C., Dorale, J.A., 2001. A high-resolution absolute-dated Late Pleistocene monsoon record from Hulu Cave, China. Science 294, 2345–2348.
Wang, Y.J., Cheng, H., Edwards, R.L., He, Y.Q., Kong, X.G., An, Z.S., Wu, J.Y., Kelly, M.J., Dykoski, A., Li, X.D., 2005. The Holocene Asian monsoon: links to solar changes and North Atlantic Climate. Science 308, 854–857.
Wang, Y.J., Cheng, H., Edwards, R.L., Kong, X.G., Shao, X.H., Chen, S.T., Wu, J.Y., Jiang, X.Y., Wang, X.F., An, Z.S., 2008. Millennial-and orbital-scale changes in the East Asian monsoon over the past 224,000 years. Nature 451, 1090–1093.
Wanner, H., Beer, J., Bütikofer, J., Crowley, T.J., Cubasch, U., Flückiger, J., Goosse, H., Grosjean, M., Joos, F., Kaplan, J.O., Küttel, M., Müller, S.A., Prentice, C., Solomina, O., Stocker, T.F., Tarasov, P., Wagner, M., Widmann, M., 2008. Mid- to Late Holocene climate change: an overview. Quatern. Sci. Rev. 27, 1791–1828.
Xiao, J.L., An, Z.S., Liu, T.S., Inouchi, Y., Kumai, H., Yoshikawa, S., Kondo, Y., 1999. East Asian monsoon variation during the last 130,000 years: evidence from the Loess Plateau of central China and Lake Biwa of Japan. Quatern. Sci. Rev. 18, 147–157.
Yuan, D.X., Cheng, H., Edwards, R.L., Dykoski, C.A., Kelly, M.J., Zhang, M.L., Qing, J.M., Lin, Y.S., Wang, Y.J., Wu, J.Y., Dorale, J.A., An, Z.S., Cai, Y.J., 2004. Timing, duration and transitions of the last interglacial Asian monsoon. Science 304, 575–578.
Zhang, R., Delworth, T.L., 2005. Simulated tropical response to a substantial weakening of the Atlantic thermohaline circulation. J. Clim. 18, 1853–1860.
Zhao, K., Wang, Y.J., Edwards, R.L., Cheng, H., Liu, D.B., Kong, X.G., Ning, Y.F., 2016. Contribution of ENSO variability to the East Asian summer monsoon in the late Holocene. Palaeogeogr. Palaeoclimatol. Palaeoecol. 449, 510–519.
Zhou, H.Y., Zhao, J.X., Wang, Q., Feng, Y.X., Tang, J., 2011. Speleothem-derived Asian summer monsoon variations in Central China, 54–46 ka. J. Quat. Sci. 26 (8), 781–790.